Thermal Design, Analysis, and Testing of a Cryogenic Optical System for Characterising the Ariel Space Telescope

Adam D. Wilkinson*[a], Robert Spry[a], Jake D. Hutchinson[a], Roy Preece[a], John-Paul Walker[a], Rebecca Holleb[a], Robert Watkins[a], Emma Ryan[a], Liam McSherry[a], Waqas Mir[a], Greg King[a], Cédric Pereira[b], David Miguel Ventura de Castro Alves[b], Fraser Clarke[a], Manuel Abreu[b], and Neil Bowles[a]

[a]Department of Physics, University of Oxford, UK
[b]Institute of Astrophysics and Space Sciences, University of Lisbon, Portugal

ABSTRACT

This paper presents developments in the thermal design and testing of the optical ground support equipment (OGSE) used to characterise the optical performance of the Ariel space telescope at payload level. As part of ESA's Cosmic Vision programme, Ariel will carry out transit spectroscopy on approximately 1,000 exoplanets over four years of operation.

To simulate a flight-like thermal environment during payload level testing, the payload is enclosed in the cryogenic test rig which provides a 35 K radiative environment. The payload is illuminated by the OGSE, which comprises an illumination module that illuminates the payload and a periscope module that steers the test beam into the payload line of sight. To enable verification of the dark current requirement in the payload's detectors ($< 1\,e^-\,pix^{-1}\,s^{-1}$), both the periscope and illumination module must be kept at 70 K.

The illumination module has a two-stage thermal design consisting of a thermally isolated optical bench and a radiative shroud constructed from low-emissivity MIRO-27 sheeting. The optical bench and radiative shield are cooled using a pair of cryocoolers connected to flexible, high-conductivity copper straps.

To de-risk the thermal design, a thermal breadboard of the illumination module has been constructed. Here, we present the thermal designs of the periscope and illumination module as well as the results of the thermal breadboarding activities. In particular, the cryocooler performance was found to be consistent with the manufacturer's specifications. The thermal performance of the flexible copper straps was characterised, and the influence of thermal interface materials on interface conductance was quantified, with 40 μm graphite foil providing approximately twice the interface conductance of direct metal-to-metal contact for heaters operating at approximately 100 °C. The dominant thermal loads acting on the illumination module shroud were identified, and the effective emissivity of a MIRO-27-based shroud was determined to be 3.5 %. Furthermore, the periscope thermal design was experimentally verified at its operational temperature of approximately 70 K, and several critical aspects of the periscope thermal design were de-risked.

Keywords: Ariel, Ground calibration, Space telescope, Optical ground support equipment (OGSE), Cryogenic testing, Thermal, TVAC

1. INTRODUCTION

1.1 The Ariel Mission

The atmospheric remote sensing infrared exoplanet large-survey (Ariel) is a European Space Agency (ESA) space telescope mission aiming to answer fundamental questions about the composition, formation, and evolution of extrasolar planetary systems. Ariel will be the first mission dedicated to performing transit/eclipse spectroscopy on a statistically significant and diverse sample of exoplanets.[1]

*adam.wilkinson@physics.ox.ac.uk; Phone +44 1865 272859

1.2 Payload Design

Ariel uses a 1 m off-axis Cassegrain telescope to feed stellar flux into two instruments: the Ariel infrared spectrometer (AIRS), which operates in the 1.95–7.80 μm range, and the fine guidance sensor (FGS), which operates in the 0.5–1.95 μm range. To ensure adequate photometric stability, low-noise (less than 1 e^- pix^{-1} s^{-1}) mercury cadmium telluride (MCT) detectors are used. These detectors can only be operated in cryogenic conditions (∼40 K).[2]

1.3 Payload Test Architecture

To achieve Ariel's goal of characterising exoplanet atmospheres, the performance of its optical design must be verified before launch at component, unit, subsystem, and payload levels. Ariel's performance will be verified at payload level in a 5 m test chamber at the Rutherford Appleton Laboratories Space (RAL Space) Instruments Test Facility using the configuration shown in Figure 1.

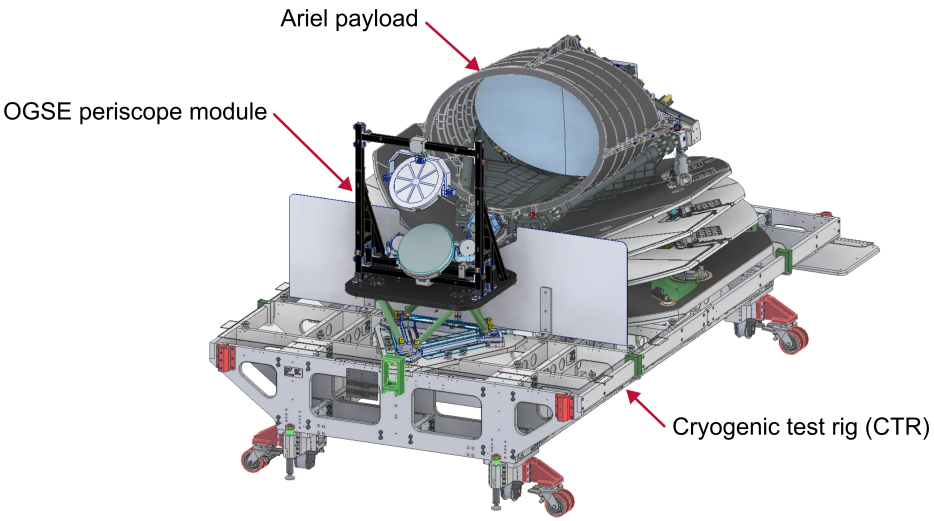

Figure 1: The CTR (shown with shroud removed), which houses the Ariel payload and the OGSE periscope module. The CTR will be housed in a 5 m vacuum chamber at RAL Space during payload level testing. A test beam will be injected into the chamber by the OGSE illumination module and will be steered into the payload by the periscope module.

To provide a flight-representative thermal environment during payload level optical and thermal testing, the payload will be enclosed in a CTR to provide a space-like radiative environment (∼35 K and vacuum). The payload's field of view (FoV) will be illuminated by the optical ground support equipment (OGSE) with a well-characterised collimated beam of light. The OGSE will provide point and extended source illumination across Ariel's spectral range, as well as providing various other operational features to check Ariel's ability to fulfil its science goals.[3]

The Ariel OGSE consists of two modules: an illumination module capable of generating both test and alignment beams across Ariel's spectral range and a periscope module which will redirect the illumination module's output into the payload's line of sight.[4]

The OGSE periscope module structural–thermal model (STM) and CTR will undergo a 'blank' test campaign at RAL Space in the summer of 2026. This paper describes the procedures for the thermal verification of the periscope STM before the blank test at RAL Space, and how those procedures will de-risk key thermal design aspects of the illumination module.

1.4 Periscope Module Thermal Design

As shown in Figure 2, the periscope module contains two 340 mm diameter mirrors in a Z-fold arrangement, which can be adjusted in tip/tilt using piezoelectric actuators. To ensure that the dark current in AIRS is less than $1\,e^{-}\,pix^{-1}\,s^{-1}$, all OGSE optics, including the periscope mirrors, must be maintained at less than 70 K.

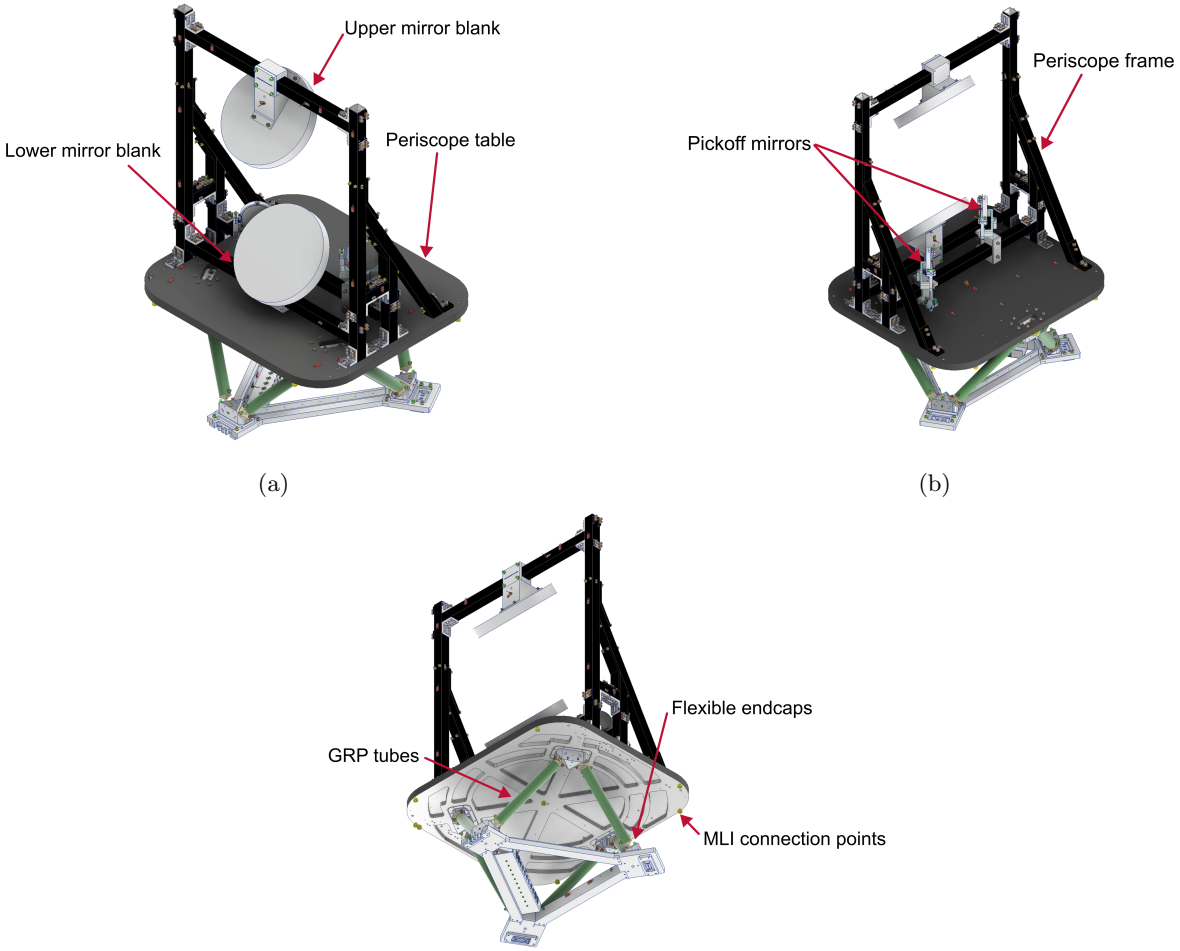

Figure 2: The OGSE periscope module in its STM configuration, showing: (a) the upper half of the periscope with the lower mirror facing forwards; (b) the upper half of the periscope with the upper mirror facing forwards, highlighting the pick-off mirrors used to guide the illumination module alignment beam; (c) the lower half of the periscope, highlighting the GRP tubes, flexible end-caps, and MLI connection points (MLI is not shown in this figure).

The periscope is a passive, radiatively cooled system. During operation within the CTR, it is mechanically supported by the CTR trolley, which is maintained at approximately room temperature (~ 293 K). The periscope and payload are enclosed by the CTR shroud which is actively cooled to 35 K, thereby establishing the radiative thermal environment for the system.

The periscope consists of two thermally distinct stages separated by a 30 mm thick aluminium table. The upper stage contains the optical assembly and is maintained at approximately 70 K, while the lower stage consists of low-conductivity glass-reinforced plastic (GRP) support legs that minimise conductive heat transfer from the CTR trolley. The underside of the periscope table is surrounded by multilayer insulation (MLI) to minimise radiative thermal coupling between the warm and cryogenic sections of the periscope structure. The upper

stage, including the table, is coated with high-emissivity black paint and functions as a radiator, emitting thermal radiation to the surrounding 35 K shroud.

Temperature control of both stages is achieved using resistive heaters mounted to the periscope table and structural frame. The heaters are operated in a closed-loop PID control system using temperature feedback from seven DT-670 silicon diode sensors and one PT-100 platinum resistance thermometer (PRT) distributed throughout the periscope assembly, in the locations shown in Figure 3. PRTs have a higher temperature sensitivity and resolution than silicon diodes at 70 K but unlike silicon diodes they require individual calibration at cryogenic temperatures as no universal calibration curve exists. Although the periscope is cooled primarily through radiation to the 35 K shroud, active heater control is used to maintain the optical assembly at its nominal operating temperature of approximately 70 K.

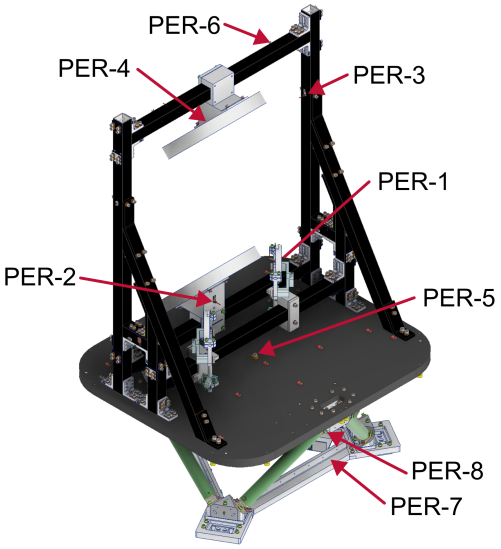

Figure 3: Temperature sensor locations on the periscope module.

Belleville washers are conical disc springs that provide a controlled spring force, making them useful in systems operating down to 70 K because they maintain a constant clamping load despite differential thermal contraction of components during cooldown. These washers are used throughout the periscope in order to maintain pre-load, and thus interface conductance, as the periscope is cooled to 70 K.[5]

The periscope STM is mechanically and thermally representative of the final deliverable configuration, differing only in that the mass-representative mirror blanks and their associated mounting hardware are used in place of the final mirrors and mirror mounts. Further details of the periscope optical design can be found in Hutchinson et al. (2026).[6]

1.5 Illumination Module Thermal Design

The illumination module (shown in Figure 4) consists of two optical benches, one remaining in ambient conditions and one cryogenic bench inside a vacuum chamber. The illumination module vacuum chamber uses a two-stage thermal architecture to maintain an optical bench operating temperature of approximately 70 K. The cryogenic optical bench is actively cooled by an SHI RDK-500B cryocooler while a radiative shroud surrounding the optical bench is cooled by a second, identical cryocooler.

Each cryocooler is connected to its respective thermal stage by flexible copper thermal straps. These straps provide a high-conductivity thermal path while accommodating differential thermal contraction from the different coefficients of thermal expansion (CTE) between components. In addition, the flexible straps attenuate the transmitted vibration from the cryocoolers, thereby reducing pointing jitter in the optics.

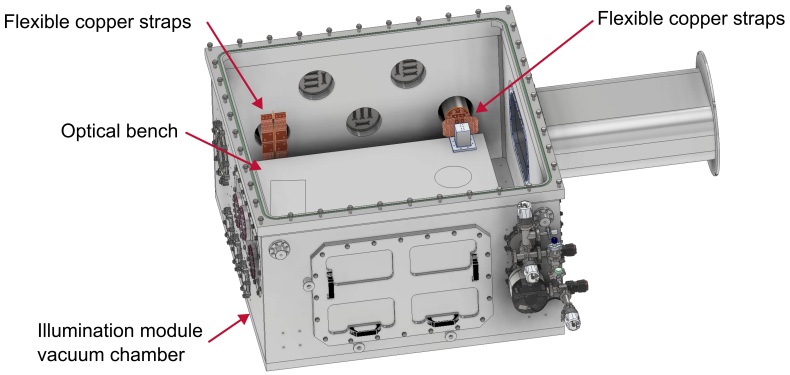

Figure 4: The illumination module chamber shown without radiative shroud and optics. Flexible copper straps connect the optical bench and radiative shroud to a pair of cryocoolers.

The radiative shroud and optical bench are independently supported by thermally insulating GRP posts. The shroud is supported from the vacuum chamber base and the optical bench is mounted on a low-vibration support structure that passes through bellows in the chamber base. This arrangement provides vibration isolation from the cryocoolers and vacuum pumps, which are mechanically interfaced to the chamber, and also minimises conductive heat transfer between cryogenic and ambient structures.

2. VERIFICATION OF THE PERISCOPE MODULE THERMAL DESIGN

2.1 Periscope Test Flow

Before delivery to RAL Space and integration into the CTR for the blank test, the periscope and associated hardware will undergo a series of preparation and testing activities, as shown in Figure 5. This paper will focus on the thermal testing of the periscope STM (highlighted in the figure). Details of future periscope testing can be found in Spry et al. (2026).[7]



Figure 5: The overall periscope test flow, with the STM thermal testing highlighted.

The first phase of periscope STM thermal testing consists of a dedicated, unit-level thermal-vacuum (TVAC) heater test campaign to characterise the performance of the proposed periscope heaters. This testing will establish the operational limits of the heaters, the effects of different thermal interface materials on interface conductance, and also assess the effects of Belleville washer configurations and pre-load conditions on transmitted heating power.

Following unit-level heater testing, the periscope will undergo an 80 °C TVAC bakeout to reduce molecular contamination and remove volatile contaminants from the assembly.

The final phase is a cryogenic TVAC test (cryotest) at the periscope's operating temperature. This test will validate the thermal and mechanical performance of the periscope under representative operating conditions and de-risk key design features, including the compliant end-cap interfaces between the GRP support tubes and the periscope table. For this test, the periscope upper half will be cooled to approximately 70 K whilst the lower half remains at room temperature to de-risk these key design features.

2.2 Unit-Level Heater Test

Unit-level heater tests were conducted to quantify the effects of thermal interface material and bolt pre-load on the thermal coupling between the periscope heaters and the hardware they are warming.

To test the heaters used on the periscope assembly, a compact radiative shroud, consisting of 5 mm sheet aluminium surrounded by single-layer insulation (SLI), was installed within a 1 m diameter thermal-vacuum chamber. As shown in Figure 6, two independent heater lines were mounted to the radiative shroud. Each line consisted of a series of Arcol AP851 resistors, identical to those used throughout the periscope module.

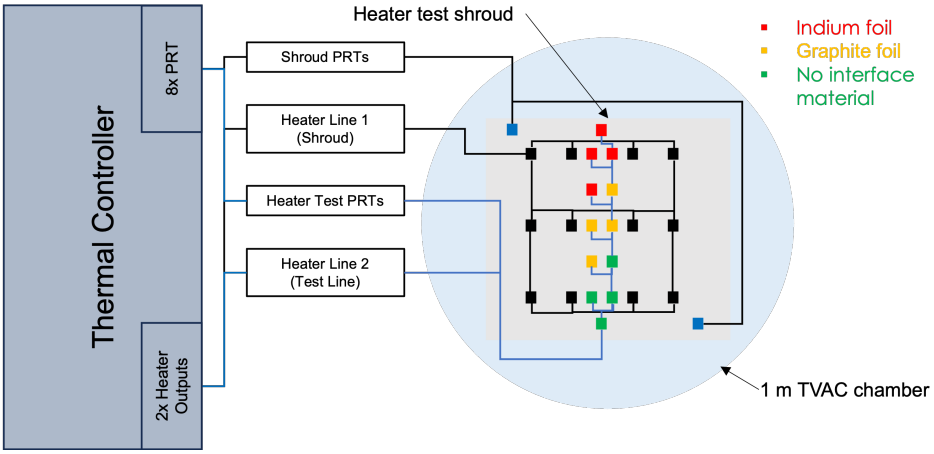

Figure 6: A schematic of the unit-level heater test facility showing the locations of each configuration of interface foil used and the locations of the shroud heaters and PRTs.

The first heater line maintained the shroud at the bakeout temperature of 80 °C throughout the test campaign. Each resistor was attached to the structure using a single Belleville washer and a bolt pre-load of 0.7 Nm to achieve 45 % deflection of the washer (best practice value) and maintain pre-load on the bolt during cooling despite the CTE offset between the bolt and the hardware.

The second heater line was used to investigate the effect of bolt pre-load and interface material on heater performance. A PRT was mounted to each resistor to measure the local temperatures of the resistor's plastic housing. The resistors were installed in one of three thermal interface configurations: without interface material (direct metal-to-metal contact), with 100 μm indium foil, or with 40 μm graphite foil. In addition, two bolt pre-load conditions, 0.7 Nm and 1.4 Nm, were evaluated, giving six unique mounting configurations. For the test, the heater power on the second line was stepped and the temperatures of the resistors were measured.

2.3 Periscope Cryostat

To support the bakeout and cryotest campaigns described in 2.1, a dual-purpose periscope cryostat, incorporating a radiative shroud, was designed and manufactured to be operated inside a 2 m diameter vacuum chamber.

As shown in Figure 7, the cryostat consists of a low-emissivity shroud thermally coupled to an RDK-500B cryocooler through a large aluminium 6061 thermal interface bar with copper side panels, and four flexible copper thermal straps. The same cryocooler and thermal interface bar are also used to provide direct cooling to the upper section of the periscope.

The shroud is $\sim$1 m^3 in volume, and consists of a 3 mm thick aluminium sheet mounted directly to the periscope table and enclosed within a 0.4 mm thick MIRO-27 low-emissivity radiation shield. The shroud is mounted to the periscope at four points, using three-way right-angled brackets. The MIRO-27 shield is thermally isolated from the aluminium sheet using low-conductivity polyether ether ketone (PEEK) bushings. During bakeout, the low-emissivity shroud reduces radiative heat loss from the periscope, and so decreases the heater power needed to keep the assembly at the prescribed bakeout temperature. During cryotest, the shroud reduces the radiative load on the periscope from the room-temperature 2 m vacuum chamber.

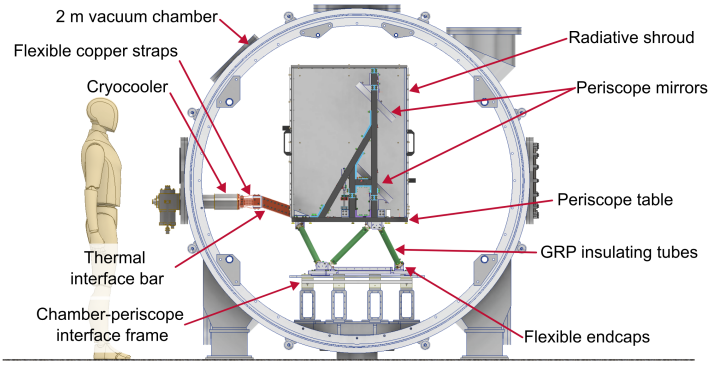

Figure 7: Experimental test setup for the periscope cryotest shown in the University of Oxford's 2 m vacuum chamber. The periscope module was housed in a custom cryostat with a MIRO-27 radiative shroud, flexible copper straps, and a cryocooler.

2.4 Periscope Bakeout

The periscope bakeout was carried out under TVAC conditions (less than 10^{-5} hPa) to remove volatile contaminants prior to cryogenic testing and was monitored by a quartz crystal microbalance (QCM) to measure the rate and quantity of molecular outgassing. Cleanliness was also monitored using molecular organic contamination (MOC) and particulate contamination (PAC) plates. Temperature control was achieved using a Lakeshore Model 336 temperature controller operating in a closed-loop PID configuration, which provided up to 150 W of heater power to heaters mounted to the periscope table and frame, while monitoring eight temperature sensors mounted to the periscope and four temperature sensors mounted to the radiative shroud. The bakeout temperature was regulated using a designated control sensor placed at the warmest section of the periscope, with the upper section of the periscope maintained at a setpoint of 80 °C throughout the test. The lower section of the periscope, which remained at room temperature during the bakeout, was baked at component level before integration with the rest of the periscope.

2.5 Periscope Cryotest

The cryotest campaign was conducted to reduce technical risk associated with key periscope design features including: performance of the flexible thermal straps, performance of the RDK-500B cryocoolers, performance of the graphite thermal interface foil, the effective emissivity of the MIRO-27 sheet mounted on sheet aluminium using PEEK bushings, and the effectiveness of using the Belleville bolting philosophy.

The periscope cryotest was done using the eight periscope temperature sensors and a further ten temperature sensors (four PRTs and six silicon diodes identical to those used on the periscope) in the locations shown in Figure 8. Measurements were taken at two thermal setpoints, first at an equilibrium temperature with only the cryocooler active, and second at a setpoint that required the periscope heaters to be active. From these measurements it was possible to calculate the conductance of the flexible copper straps, the effective emissivity of the shroud, the power as a function of temperature of the RDK-500B cryocooler, and the gradients across the radiative shroud.

3. DE-RISKING OF THE ILLUMINATION MODULE THERMAL DESIGN

The verification of the periscope thermal design and the associated cryostat test campaign also gave an opportunity to reduce technical risk associated with the illumination module thermal architecture. The radiative shroud used in the illumination module is comparable both in size ($\sim$1 m^3) and function to that used in the periscope cryostat. In both cases, the shroud is exposed to a room-temperature vacuum chamber environment ($\sim$300 K) while enclosing optical components that must operate at approximately 70 K. Therefore, the thermal behaviour of the periscope cryostat is highly representative of that expected for the illumination module, except for the extra cooling power available to the illumination module due to the use of a second cryocooler.

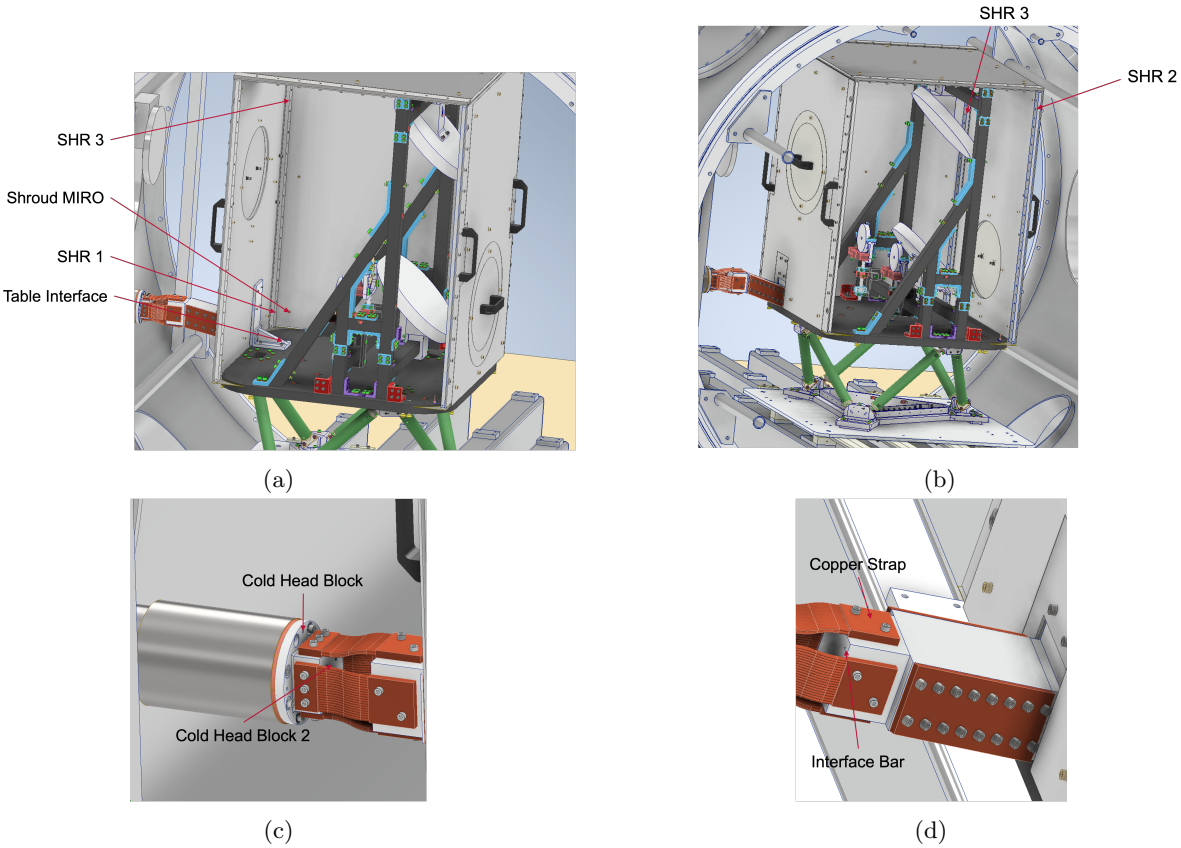

Figure 8: Arrangement of the temperature sensors during the periscope cryotest. The sensor labels correspond to the identifiers used throughout Section 5.

In addition, the RDK-500B cryocooler used in the periscope cryostat is identical to the cryocoolers which will be used for cooling the illumination module optical bench and radiative shroud. The flexible copper thermal straps used in both systems are of similar geometry, material, and thermal function, enabling direct assessment of their cryogenic performance and interface conductance under representative operating conditions during use in the periscope cryostat.

Finally, the resistive heaters, temperature sensors and thermal controllers employed on the periscope are identical to those intended for use throughout the illumination module. Verification of the performance of these heaters, together with the cryocoolers, thermal straps, and radiative shielding, within a representative thermal environment provides a valuable opportunity to validate key elements of the illumination module design and significantly reduce technical risk prior to finalising the thermal design of the illumination module.

4. ANALYSIS

4.1 Periscope Thermal Design Analysis

A Simulink thermal model of the periscope cryostat was developed to predict the cool-down time of the system, the equilibrium temperature of the periscope, and the magnitude of parasitic heat loads present during testing.

Figure 9 shows a block diagram of the thermal model. The periscope shroud is exposed to a 293 K radiative environment representing the vacuum chamber walls, while the upper section of the periscope is enclosed by the shroud, except the underside of the periscope table, which is protected by MLI. These radiative thermal loads are represented by two radiative heat transfer blocks, each modelling the heat exchange between parallel surfaces of known emissivity. Conductive heat transfer between the periscope and the ambient environment is represented

by a conductive heat transfer block modelling the GRP support tubes using the material's thermal conductivity and geometric dimensions of the supports.

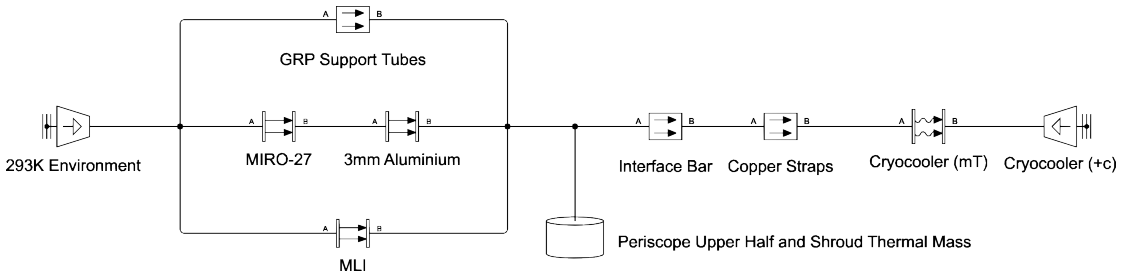

Figure 9: The initial Simulink thermal model used to predict the cool-down time, and periscope equilibrium temperature of the periscope cryotest.

The periscope is thermally linked to a simplified model of the cryocooler. The cryocooler is represented by a temperature-dependent heat sink based on a linear approximation of the RDK-500B capacity map, expressed as $Q = mT + c$, where Q is the available cooling power, T is the cold-head temperature, and m and c are fitted to the RDK-500B capacity map. The thermal connection between the periscope and cryocooler is modelled using two additional conductive heat transfer blocks representing the aluminium thermal interface bar and the flexible copper thermal straps. The equations governing this block diagram, as well as a more detailed description of the RDK-500B model, can be found in Appendix A.

This model makes several assumptions. Firstly, the chamber walls were modelled as a black body with an emissivity of 100 %, the emissivity of the MIRO-27 was modelled as 3 %, the periscope table MLI as 2 %, and the aluminium of the shroud walls as 20 %. These values, especially that of the MIRO-27 surface, are not well characterised in the available literature and it was one of the objectives of this test campaign to assess the validity of these assumptions during test.

Secondly, perfect thermal contact conductance was assumed at all mechanical interfaces. This simplification was because of the inherent difficulty of accurately modelling interface conductance without extensive empirical data.

Finally, the periscope and shroud were assumed to behave as a single isothermal thermal mass with a uniform specific heat capacity. This assumption was considered reasonable because a substantial fraction of the assembly is constructed from aluminium and mounted to a thick aluminium table, which was expected to minimise temperature gradients throughout the structure.

The model predicted that the total parasitic loads on the system would be 42 W and that the periscope would reach an equilibrium temperature of 60 K after 180 hours.

5. RESULTS

5.1 Unit-Level Heater Test

The results of the unit-level heater test are shown in Figure 10. At the start of the test, a maximum temperature gradient of 2 °C was observed across the shroud. This value was taken as the effective resolution of the experiment when comparing the performance of different heater mounting configurations.

The heater power is presented as a percentage on the right-hand axis of Figure 10. A heater power of 100 % corresponds either to a maximum thermal controller total heater power of 26.4 W, or to a maximum total heater power of 50 W, as indicated on the figure. The second heater line consisted of twelve 2.2 Ω resistors connected in series.

Across the full range of powers tested, the lowest resistor shell temperatures were measured when using graphite foil with a pre-load of 0.7 Nm. However, the performance of both graphite foil and indium foil was equivalent within the experimental uncertainty, irrespective of pre-load. Configurations with no thermal interface

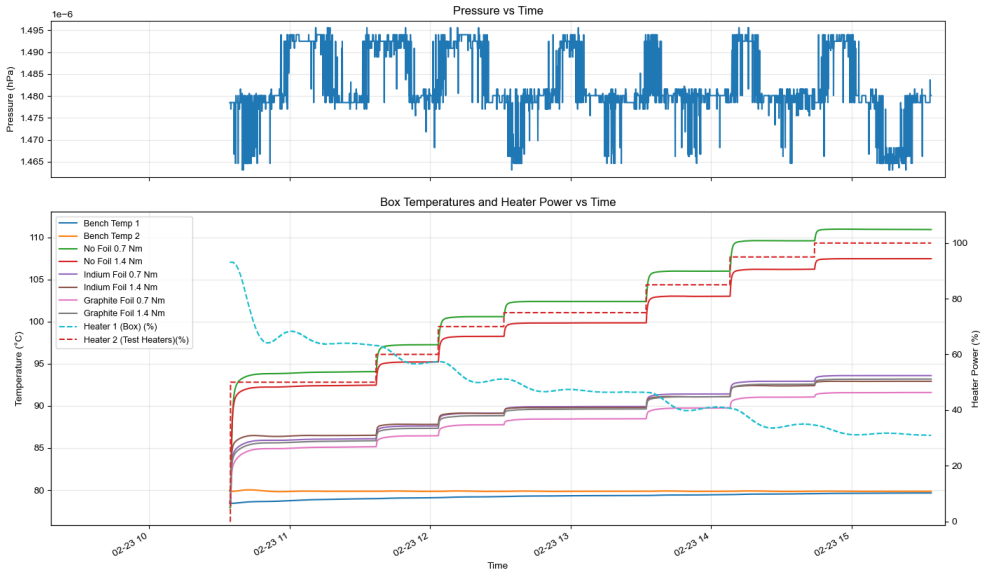

(a)

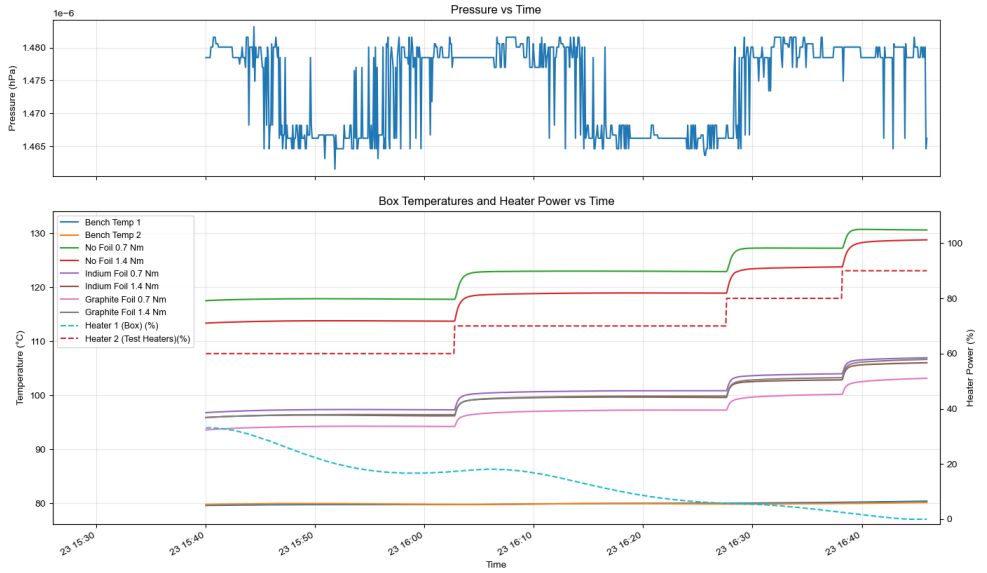

(b)

Figure 10: The results of the unit-level heater test showing: (a) the results when a maximum heating power of 26.4 W was available, and (b) the results when that maximum power was increased to 50 W.

material, however, showed significantly poorer performance, resulting in resistor temperatures approximately 20 °C higher than those measured for the graphite foil configuration.

At a total heating power of 50 W, each individual resistor received 4.1 W of individual heating power, the bench was maintained at 80 °C, the 0.7 Nm pre-loaded graphite foil resistor had a temperature of 105 °C, and the 1.4 Nm pre-loaded resistor without interface foil had a temperature of 130 °C. This corresponds to an interface conductance of 0.16 W/K for the graphite foil and 0.08 W/K for no interface foil.

Given the comparable thermal performance of graphite foil and indium foil, graphite foil was selected as the

preferred thermal interface material for the OGSE because of its lower cost and simpler integration. Furthermore, as a resistor temperature of 105 °C remained comfortably within the manufacturer's derating limits, a maximum operating power of 4.1 W per resistor was adopted for subsequent use of these heaters within the OGSE.

5.2 Periscope Bakeout

Shown in Figure 11 are the results of the periscope bakeout campaign. During the bakeout, the periscope was maintained at ∼80 °C and the pressure in the chamber remained below 1×10^{-5} hPa. The total duration of the bakeout was 144 hours at which point the European Cooperation for Space Standardization (ECSS) stopping criterion for QCM linearity had been met.[8]

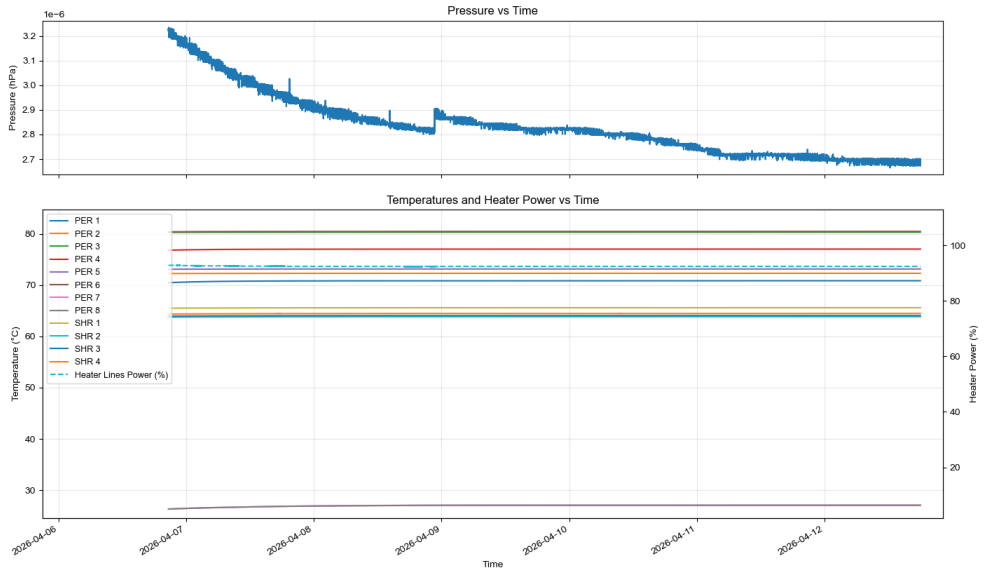

Figure 11: The results of the periscope bakeout showing data from the temperature sensors, heater lines, and pressure gauge during bakeout.

Due to the imposed heater operating limits, a maximum total heating power of 53.9 W was available during the bakeout. To maintain an equilibrium temperature of ∼80 °C, the thermal controller operated at 92 % of the total heater available, corresponding to 49.6 W.

Assuming an effective emissivity of 2 % for the MLI-covered underside of the periscope table (as this is better characterised in literature) and a uniform shroud temperature of 65 °C, the measured equilibrium heater power of 49.6 W implies a total parasitic heat load of the same magnitude. A parasitic heat load of 49.6 W suggests that the MIRO-27 has an emissivity of 3.5 %.

5.3 First Periscope Cryotest Root-Cause Analysis

After the bakeout, the flexible copper straps were connected to the cryocooler, and the periscope was cooled. The first cryogenic test did not achieve the periscope's operational temperature, indicating that the initial thermal model had not accurately predicted the thermal behaviour of the cryostat. Shown in Figure 12 are the results of the first cryotest.

To better understand the discrepancy between the model predictions and the measured performance, a retrieval model was developed. In this model, both the incident parasitic heat load and the conductance of the thermal interface bar and flexible copper straps were adjusted to reproduce the temperatures measured across several points (cold head block, interface bar, table interface, and PER-5 as per Figure 8) along the cryostat's thermal path during the test. The retrieval model indicated that approximately 99 W of parasitic heat load was

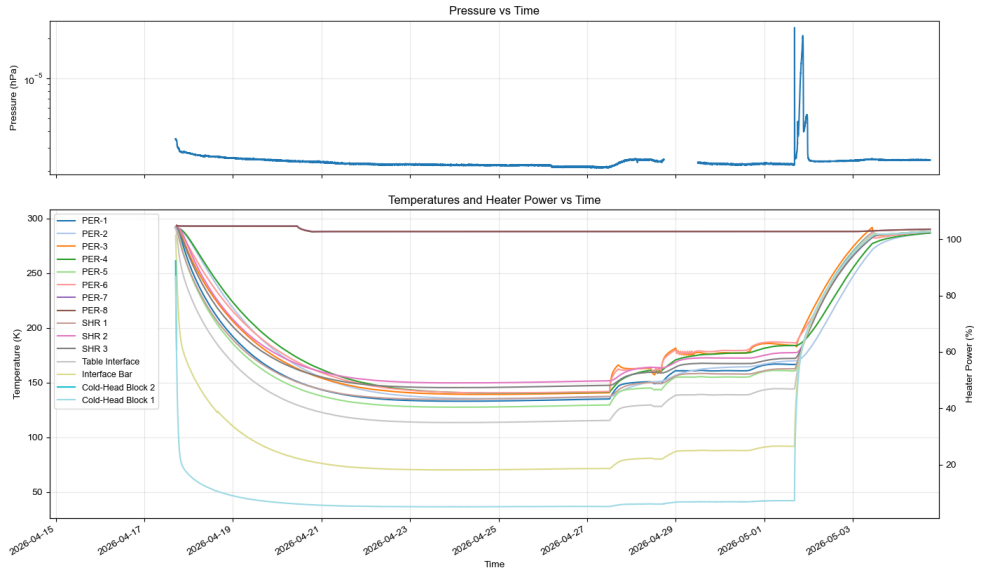

Figure 12: The results from the first periscope cryotest showing the initial cooldown, the first plateau at equilibrium (no heaters), the two following plateaus at higher temperatures (using the periscope heaters), and finally warmup.

incident on the cryostat during the first cryotest, representing an increase of 57 W relative to the prediction of the initial thermal model.

To determine the source of these additional heat loads, a more detailed thermal analysis was carried out using Simulink, and the block diagram is shown in Figure 13. This analysis followed the methods of the original thermal model but relaxed several simplifying assumptions and explicitly accounted for previously neglected heat transfer paths. Potential contributors to the increased parasitic load included: exposed regions of the 3 mm aluminium shroud panel and periscope hexapod assembly that were not covered by MIRO-27 shielding; radiative loading on the uninsulated cryocooler, thermal interface bar, and flexible copper straps; and radiative loading associated with the GRP support tubes and electrical wiring. The results of this analysis are summarised in Table 1.

Table 1: Parasitic heat load contributions identified during the root-cause analysis of the first cryotest.

Parasitic Load	**Power (W)**
Radiative load on MIRO-27	34.0
Radiative load on exposed sections of the 3 mm panel	28.0
Radiative load on temperature sensors and heater wiring	6.0
Radiative load on periscope table MLI	5.8
Radiative load on thermal bar and flexible copper links	5.0
Radiative load on GRP tubes	4.7
Radiative load on exposed hexapod endcaps	3.5
Radiative load on exposed hexapod interface blocks	2.3
Total	**89.3**

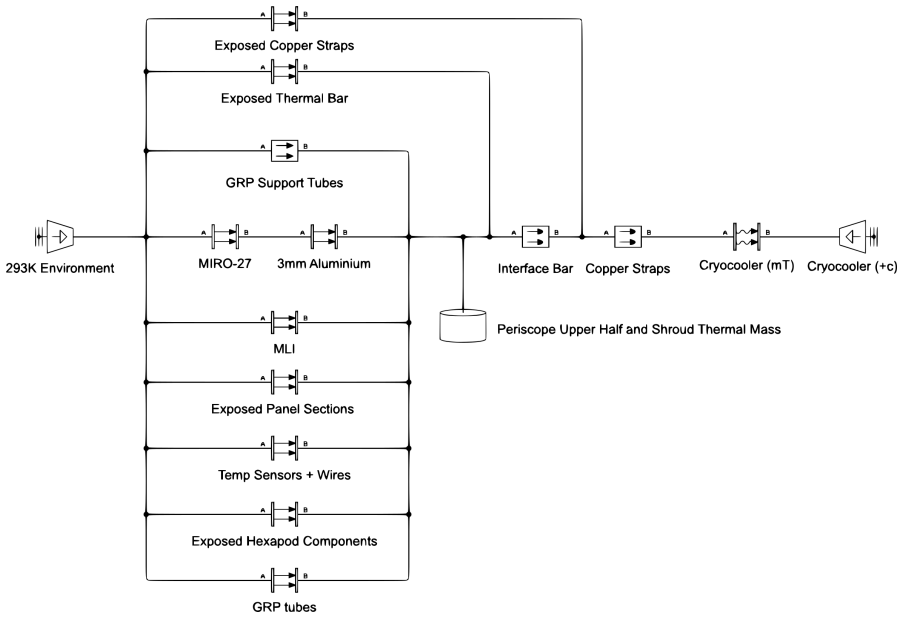

Figure 13: Block diagram of a more detailed thermal model used to characterise the previously neglected heat paths in the periscope cryostat in order to analyse their magnitudes and diagnose the increased parasitic load.

The root-cause analysis was able to account for approximately 89 W of the 99 W parasitic load predicted by the retrieval model. Given the uncertainty in the emissivity values used in the analysis, this level of agreement was considered satisfactory, as small changes in the emissivities used could account for the entirety of the missing parasitic loads. For example, increasing the assumed emissivity of the aluminium surfaces from 20 % to 26 % would account for the remaining discrepancy. Consequently, the updated thermal model was considered sufficiently representative to support planning of a second cryogenic test of the periscope.

In addition to the increased parasitic heat load, the retrieval model suggested that the conductance of the thermal interface bar and flexible copper straps was significantly lower than originally thought. The measured and expected conductances are compared in Table 2.

Table 2: Measured (retrieval model) and expected (root-cause analysis model) thermal conductances of conductive thermal links.

Component	**Measured Conductivity (W/K)**	**Expected Conductivity (W/K)**
Thermal interface bar	2.2	5.0
Flexible copper straps	2.7	4.1

5.4 Changes Before Second Cryotest

To reduce the parasitic heat loads identified during the root-cause analysis, several modifications were made before the second cryogenic test. First, a tent made from 0.15 mm aluminised Mylar SLI was installed around the radiative shroud. The exposed hexapod components, thermal interface bar, flexible copper straps, and cryocooler were each surrounded by SLI and additional SLI sheaths were fitted around the final ∼10 cm of the GRP support tubes and temperature sensor wiring to reduce radiative heat transfer. This approach was used because the majority of the temperature gradient within these components was expected to occur close to their interfaces with the cryogenic hardware.

To improve the conductance of the cooling path, bolt pre-loads were tripled, requiring a corresponding increase in the number of Belleville washers used at each interface. Stainless steel distribution plates were introduced at the interfaces between the flexible copper straps and the thermal interface bar to provide a more uniform distribution of the applied pre-load and so improve thermal contact conductance across the interface. The cryostat before the first and second cryotests is shown in Figure 14.

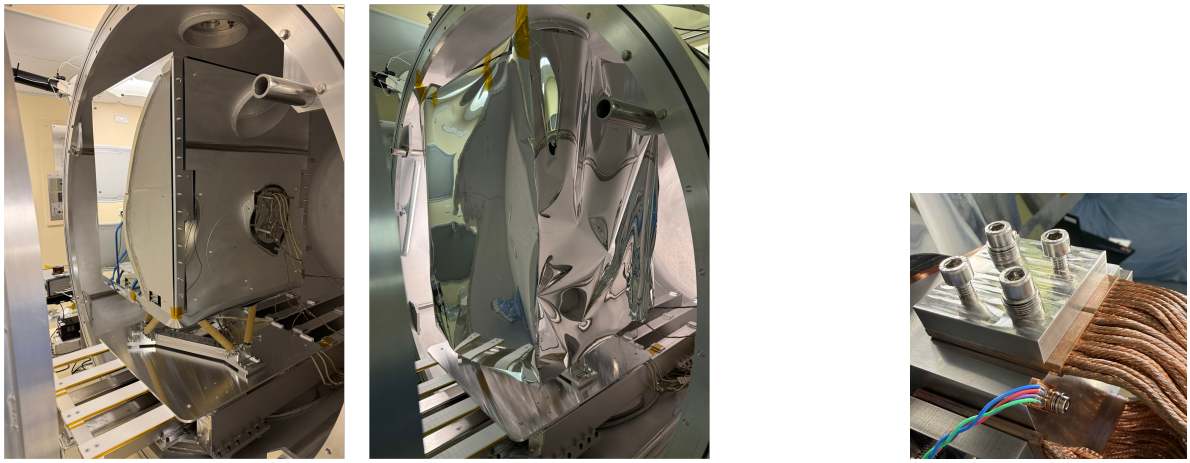

(a) (b)

Figure 14: (a) The custom periscope cryostat shown inside the 2 m chamber before the first (left) and second (right) cryotests commenced. (b) The stainless steel distribution plates added to increase interface conductance on the copper straps.

5.5 Periscope Cryotest Results

The results of the second cryotest are shown in Figure 15. During the test, the table interface bracket, which is integrated directly into the periscope table, reached a temperature of 70 K while the centre of the periscope table stabilised at approximately 80 K.

The total parasitic heat load was reduced by approximately 28 W relative to the first cryotest, showing the effectiveness of the additional SLI in reducing radiative heat transfer to the cryogenic hardware.

The measured conductance of the flexible copper straps increased to 4.6 W/K, which is approximately 70 % greater compared to the first cryotest. The conductance of the thermal interface bar increased by only 3.5 %. These results indicate that improving the uniformity of compression across the flexible copper strap end fittings produced a substantial increase in thermal contact conductance while the increased bolt pre-load alone provided only a marginal improvement.

6. CONCLUSIONS

6.1 Overview

A programme of heater characterisation, thermal-vacuum bakeout, and cryogenic testing was conducted to verify the thermal design of the Ariel OGSE periscope and to investigate key elements of the illumination module thermal architecture. After making modifications identified through root-cause analysis of the initial cryogenic test, the second cryotest successfully achieved the primary thermal objective of the campaign: the periscope table interface bracket reached the target operating temperature of 70 K while the lower half of the periscope remained at 300 K. The campaign also provided valuable data for thermal model correlation and allowed the identification of several key design improvements for both the periscope cryostat and illumination module. The main conclusions of this work are summarised below.

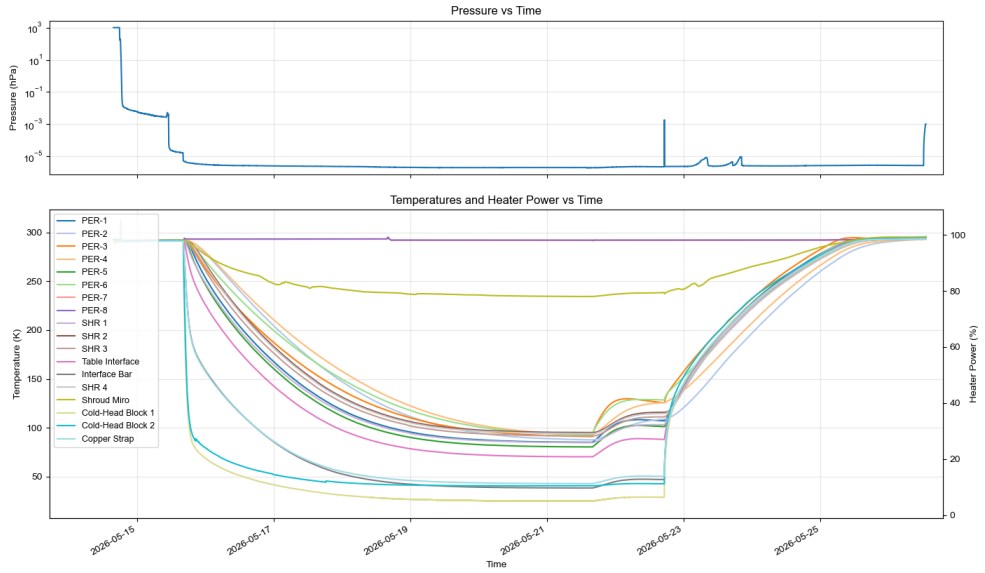

Figure 15: The results from the second periscope cryotest showing the initial cooldown, the first equilibrium plateau (no heaters), the second plateau using the periscope heaters, and finally warmup.

6.2 Flexible Thermal Straps

The cryogenic test campaign showed that the performance of the flexible copper thermal straps is sufficient for use in the OGSE but remains strongly dependent on the quality of the mechanical interfaces. Improved load distribution at the strap end-fittings gave a substantial increase in thermal conductance, highlighting the importance of interface design in cryogenic thermal links.

6.3 Cryocooler Performance

The measured cooling performance of the RDK-500B cryocooler was consistent with expectations and matched the manufacturer's capacity map closely when the parasitic heat loads acting on the system were correctly accounted for. The test campaign provided valuable data for thermal model correlation and improved understanding of the cryostat thermal balance.

6.4 Graphite Thermal Interface Foil

Graphite foil almost doubled the thermal interface conductance relative to direct metal-to-metal interfacing. Its performance was comparable to that of indium foil while offering advantages in cost, handling, and integration. Consequently, graphite foil was adopted as the preferred thermal interface material for the OGSE.

6.5 Two-Stage Radiative Shroud

Root-cause analysis of the first cryotest showed that radiative heat loads were the dominant contributor to thermal performance shortfall. The effectiveness of the additional SLI shielding added for the second cryotest suggests that a two-stage radiative shielding approach is likely to be required for the illumination module to achieve the desired operating temperatures.

Overall, the cryogenic test campaign successfully reduced technical risk associated with the periscope design. The thermoelastic integrity of the flexible end-cap assemblies was validated, the selected materials and electronics were shown to be suitable for cryogenic operation, and several important design lessons were identified for the development of the illumination module.

APPENDIX A. THERMAL MODEL EQUATIONS

A.1 Radiative Heat Transfer Block

The radiative heat transfer block calculates the net radiative heat transfer between two large, parallel plates A and B as:[9]

$$Q = kA\left(T_A^4 - T_B^4\right),$$

where:

- Q is the rate of heat transfer by radiation,
- k is the radiation heat transfer coefficient,
- A is the surface area of the emitting body,
- T_A and T_B are the absolute temperatures of the two bodies.

$$k = \frac{\sigma}{\dfrac{1}{\varepsilon_1} + \dfrac{1}{\varepsilon_2} - 1},$$

where:

- σ is the Stefan–Boltzmann constant,
- ε_1 is the emissivity of the emitting surface,
- ε_2 is the emissivity of the receiving surface.

A.2 Conductive Heat Transfer Block

The conductive heat transfer block represents heat transfer by conduction through a homogeneous material. For a flat surface, the rate of heat transfer is described by Fourier's law:[10]

$$Q = k\frac{A}{D}\left(T_A - T_B\right),$$

where:

- Q is the rate of heat transfer by conduction,
- k is the thermal conductivity of the material,
- A is the cross-sectional area normal to the direction of heat flow,
- D is the material thickness,
- T_A is the temperature of layer A,
- T_B is the temperature of layer B.

A.3 RDK-500B Cryocooler Model

A convective heat transfer block, and a fixed temperature node were used to provide a linear model of the RDK-500B's cooling power.

The convective heat transfer block represents heat transfer between two bodies through the motion of a fluid. The rate of convective heat transfer is described by:[11]

$$Q = kA\left(T_A - T_B\right),$$

where:

- Q is the rate of heat transfer by convection,
- k is the convective heat transfer coefficient,
- A is the surface area through which heat is transferred,
- T_A and T_B are the temperatures of the two bodies.

By introducing a fixed temperature node, we hold T_B constant, making our equation:

$$Q = mT + c$$

where:

- Q is the temperature-dependent rate of heat transfer that the RDK-500B is capable of.
- $m = kAT_A$ is linearly dependent with temperature,
- $c = -kAT_B$ is a constant.

By inputting $A = 1$, we can fit values of k and T_B which linearly approximate the RDK-500B temperature-dependent capacity map.

ACKNOWLEDGMENTS

The University of Oxford's work was funded by a grant from UKSA. The authors from the University of Lisbon/IA were funded by Fundação para as Ciências e Tecnologias (FCT) through the research grants UIDB/04434/2020 DOI: 10.54499/UIDB/04434/2020 and UIDP/04434/2020 DOI: 10.54499/UIDP/04434/2020 and by the Portuguese Space Agency in the framework of the PRODEX Programme with the European Space Agency (ESA) under contract number PEA 4000129411.

REFERENCES

[1] Tinetti, G. et al., "Ariel definition study report," *ESA Document ESA/SCI (2020)* **1** (2020).

[2] Eccleston, P., Caldwell, A., Bishop, G., Desjonqueres, L., Drummond, R., Davidson, A., Whalley, M., Caldwell, M., Pearson, C., Simpson, C., et al., "The ariel payload design post-pdr," in [*Space Telescopes and Instrumentation 2024: Optical, Infrared, and Millimeter Wave*], **13092**, 435–455, SPIE (2024).

[3] Tunarli, E. and Tustain, S., "The conceptual design and analysis of the cryogenic test rig for the ariel payload module," 2020 International Conference on Environmental Systems (2020).

[4] Spry, R., Abreu, M., Nowicki, K., Bowles, N., Rashman, M., Pereira, C., Hutchinson, J., de Castro Alves, D. M. V., Evans, R., Watkins, R., et al., "Cryogenic testing of the integrated ariel space telescope: design of the optical test equipment," in [*Space Telescopes and Instrumentation 2024: Optical, Infrared, and Millimeter Wave*], **13092**, 1668–1684, SPIE (2024).

[5] Davet, G. P., "Using belleville springs to maintain bolt preload," *Solon Manufacturing, Co., Chardon, OH* (1997).

[6] Hutchinson, J., Spry, R., Wilkinson, A., Pereira, C., Walker, J.-P., et al., "Optomechanical design of a broadband cryogenic optical system for ground testing of the ariel payload," in [*Space Telescopes and Instrumentation 2026: Advances in Optical and Mechanical Technologies for Telescopes and Instrumentation VII*], SPIE (2026).

[7] Spry, R., Hutchinson, J., Preece, R., Wilkinson, A., Walker, J.-P., Watkins, R., Holleb, R., Ryan, E., Pereira, C., et al., "Verification methods for the ariel optical ground support equipment," in [*Space Telescopes and Instrumentation 2026: Modeling, Systems Engineering, and Project Management for Astronomy XII*], SPIE (2026).

[8] de Heij, P., Rampini, R., and Semprimoschnig, C., "Analysis of Bake-out Monitoring Data," (Jan. 2015).

[9] MathWorks, "Radiative heat transfer." https://www.mathworks.com/help/simscape/ref/radiativeheattransfer.html (2026). Accessed 17 June 2026.

[10] MathWorks, "Conductive heat transfer." https://www.mathworks.com/help/simscape/ref/conductiveheattransfer.html (2026). Accessed 17 June 2026.

[11] MathWorks, "Convective heat transfer." https://www.mathworks.com/help/simscape/ref/convectiveheattransfer.html (2026). Accessed 17 June 2026.